Preequilibrium to evaporation residues: Dynamical approach to intermediate energy nucleus-nucleus collisions

K. Krishan,* P. Wagner, J. P. Coffin, and F. Rami
Centre de Recherches Nucléaires, Boîte Postale 20, F-67037 Strasbourg CEDEX, France

S. Bhattacharya
Variable Energy Cyclotron Centre, 1/AF, Bidhan Nagar, Calcutta 700 064, India
(Received 10 October 1991)

Dynamical evolution of the nucleus-nucleus collisions in the Fermi energy domain is followed from the point of interaction to the evaporation residues on an event-by-event basis by a Monte Carlo simulation technique. The complete reaction process comprises two phases: (i) the preequilibrium phase and (ii) the evaporation phase. The initial preequilibrium phase leads to the formation of an incompletely fused composite that, assumed to be thermally equilibrated, subsequently decays leading to final residues. The calculations are parameter free. The calculated inclusive residue charge distribution, exclusive proton and α-particle spectra, and other physical observables for the reaction $^{40}Ar+^{24}Mg$ and $^{40}Ar+^{13}C$ at 1100 MeV are compared with the respective experimental data. The theoretical predictions are found to be in good agreement with the experimental results.

PACS number(s): 25.70.−z, 25.70.Jj

I. INTRODUCTION

One of the basic motivations behind the theoretical and experimental studies of nuclear reactions using nucleus-nucleus collisions is to obtain a complete insight into the gradual evolution of the reaction mechanism from the point of interaction to the final stage of the reactions. It is now established that in nucleus-nucleus collisions with incident energies less than 10 MeV/nucleon the complete fusion process is the dominant mode of reaction. In such a process, the whole of the incoming linear momentum and available energy is deposited into the compound nucleus which then fissions or deexcites through statistical evaporation, depending on whether the composite is heavy or light. With increase in the incident energy $E/A > 10$ MeV/nucleon, the phenomenon of incomplete fusion starts showing up and eventually takes over the complete fusion process [1,2]. In the incomplete fusion process, a part of the target and the projectile fuse together and there is incomplete linear momentum transfer, for which "universal" energy dependences have been suggested on the basis of several calculations [3]. The emission of light particles in the initial stage of the reaction carries away linear momentum and energy from the incompletely fused system [4–7]. This incompletely fused composite then deexcites through statistical emission or undergoes fission. So, the scenario for the nucleus-nucleus reactions with energies well above the Coulomb barrier is the following: Initially, there is a preequilibrium phase when a number of light particles are emitted which carry away energy, linear momentum, and angular momentum and an incompletely fused composite is formed; in the second phase this highly excited composite deexcites through statistical processes leading to the final residues. In the forward direction, the particle spectra from the preequilibrium and the evaporation phases are contaminated with the contributions from other direct reaction mechanisms, whereas at the backward angles the particle spectra are predominantly from the preequilibrium emission. For the inverse kinematical reactions, the situation is more favorable to observe the uncontaminated preequilibrium particle spectra at the backward angles. However, at the forward angles it is very much necessary to separate the preequilibrium and the evaporation components in the light particle spectra to have a proper understanding of the reaction mechanism.

From the theoretical standpoint, there has been no systematic attempt, to our knowledge, to study the complete dynamical evolution of the incomplete fusion process starting from the initial preequilibrium phase to the final decay of the incompletely fused composite. Landau-Vlasov calculations, which have been quite successful in explaining many of the experimentally observed quantities in the intermediate energy domain, are often prohibitive because of their inherent complexity as well as their computational time requirements. Moreover, a large amount of the experimental data concerning the emission of light particles and clusters at various stages of the reaction cannot be explained in the framework of the model, as it is not clear how to determine the precise nature of emission (nucleon, light particles, and clusters) in such calculations [8]. However, a proper understanding of the light particle emission is crucial for complete insight into the reaction mechanism of such processes. Therefore, several alternative attempts have been made in recent years to explain the light particle emission from the incompletely fused composite where the initial mass num-

*Permanent address: Variable Energy Cyclotron Centre, Calcutta 700 064, India.

ber and the excitation energy of the composite have been estimated in an average manner, either from phenomenological considerations or from rigorous Landau-Vlasov calculations [8]. In the present paper, we report a fully dynamical calculation of the evolution of the nucleus-nucleus collision process in the Fermi energy domain where the initial preequilibrium phase is followed by the evaporation of the incompletely fused composite on an event-by-event basis using a Monte Carlo simulation technique. At the end of the first phase there is a highly excited incompletely fused composite whose mass, charge, velocity, and excitation energy are known. Also known are the velocities of the preequilibrium nucleons emitted during this phase. In the next phase this incompletely fused composite is allowed to decay. There is no free parameter involved in the whole calculation from the point of contact to the final formation of residues. The reaction products for each event, i.e., light particles as well as the heavy residues, are put into different energy and angular bins from which the cross sections corresponding to various observables are estimated. The model has already been applied for the reaction $^{40}Ar+^{24}Mg$ at 1100 MeV and the predictions of the model have been found to be in good agreement with the experimental data. In the present paper, we report comprehensive theoretical calculations for the reaction $^{40}Ar+^{13}C$ at 1100 MeV and for a few observables of the reaction $^{40}Ar+^{24}Mg$ at 1100 MeV for the sake of completeness, and confront our calculated results with the experimental data.

The paper is arranged as follows. The description of the model is given in Sec. II; Sec. III contains the results and discussions; and, finally, the summary and conclusions are given in Sec. IV.

II. DESCRIPTION OF THE MODEL

The model basically consists of two parts: (i) The calculation of the preequilibrium phase and (ii) the calculation of the evaporation phase. In the preequilibrium phase, we follow the time evolution of the dinuclear complex formed in the nucleus-nucleus collision until the preequilibrium emission is over and an incompletely fused composite is formed. In the next phase, this composite, assumed to be fully thermalized, is allowed to decay by emitting light particles and clusters leaving behind the final residue.

A. Preequilibrium phase

1. The dynamics

The time evolution of the initial dinuclear complex in the preequilibrium phase of the reaction is calculated using classical trajectories obtained by solving Euler-Lagrange equations. In the trajectory calculation the conservative forces are the nuclear proximity and the Coulomb forces; the nonconservative frictional forces are generated self-consistently using stochastic nucleon exchanges. The trajectory calculation is started at an internuclear surface-to-surface separation of 3.74 fm where the densities of the colliding nuclei start overlapping, and is stopped at the time when there is no further preequilibrium emission. This time, typically $\sim$ 50 fm/c, corresponds to the internuclear distance of $\sim$2 fm; after this time the system is assumed to be thermalized.

2. The preequilibrium emission

We follow a generalized version of the promptly emitted particle (PEP) model [9] for the calculation of preequilibrium emission. When the densities of the colliding nuclei start overlapping, a window is formed at the interface through which nucleons can be stochastically exchanged between the reactants. The exchanged nucleon in the recipient has its energy boosted by the coupling of the intrinsic Fermi velocity and the nuclear relative velocity. If nucleus A is the donor and B is the recipient, then the energy of the transferred nucleon ε_b in the nucleus B is

$$\varepsilon_b = \tfrac{1}{2} m (\mathbf{v}_a + \mathbf{v}_{\rm rel})^2 , \tag{1}$$

where m is nucleon mass, $\mathbf{v}_a$ its intrinsic velocity in A, and $\mathbf{v}_{\rm rel}$ is the nuclear relative velocity. A similar case is if the nucleon is exchanged from nucleus B to nucleus A. The transferred nucleon is to overcome a barrier at the interface: Coulomb plus nuclear for the protons and only nuclear for the neutrons. The effect of driving forces, caused by the potential energy surfaces, on the nucleon transfer has been properly taken care of. We use a shell corrected macroscopic driving force, calculated from the liquid drop model. The effect of the driving force is essentially to change the chemical potential, i.e., Fermi energies. This favors the nucleon transfer in the forward/backward direction depending on its sign. The number of particles transferred from nucleus A to nucleus B (N_{AB}) at an instant of time t between the time interval t and $t+\Delta t$ is given by

$$N_{AB}(t)\Delta t = \mathcal{A}(t)\eta(\mathbf{v}_a + \mathbf{v}_{\rm rel}) f(\varepsilon_A, T_A)\bar{f}(\varepsilon_B, T_B)\tau \Delta t , \tag{2}$$

where $\mathcal{A}(t)$ is the window area at time t; η is the bulk flux; f, $\bar{f}$ are the occupancies and the unoccupancies in nucleus A and nucleus B having instantaneous temperatures T_A and T_B, respectively; and τ is the barrier penetration factor calculated using Hill-Wheeler formula assuming the barrier to be inverted parabola in the neighborhood of its maximum. The particle transfer from nucleus B to nucleus A at an instant of time can be calculated in a similar fashion. The time step Δt is chosen in such a way that the calculated flux $N_{AB}(t)\Delta t$ between time t and $t+\Delta t$ is small compared to unity. A random number is then generated, and if $N_{AB}\Delta t$ is greater than or equal to this number, a nucleon transfer is realized from the donor to the recipient. The exchanged flux gives rise to hole excitations in the donor and the absorbed part of the flux gives rise to particle excitations in the recipient. The total excitation energy of the nucleus A at time $t=(N\Delta t)$ is given by

$$E_A^*(t) = \sum_{n=1}^{N} [\Theta(N_{AB}\Delta t - R_n)\Delta E_h^A + \Theta(N_{BA}\Delta t - R_n')\Delta E_p^A] - \varepsilon_{\rm PEP} , \tag{3}$$

where Θ is the step function, R_n, R_n' are the random numbers generated at the nth time step, and ΔE_h^A and ΔE_p^A are the hole and particle excitations per nucleon transfer, respectively. The quantities ΔE_h^A and ΔE_p^A are defined as follows:

$$\Delta E_h^A = E_F - \tfrac{1}{2} m v_a^2 , \tag{4a}$$

$$\Delta E_p^A = \tfrac{1}{2} m (\mathbf{v}_{\rm rel} + \mathbf{v}_b)^2 - E_F + \omega , \tag{4b}$$

where E_F is the Fermi energy and ω is the driving force per nucleon transfer. The quantity $\varepsilon_{\rm PEP}$ corresponds to the total energy of the nucleons emitted in the continuum until the instant t, which will be discussed later in the text. The excitation energy $E_B^*(t)$ of the nucleus B is calculated in a similar way. The temperature $T_{A,B}(t)$ of the reactants at any instant of time t is given by

$$T_{A,B}(t) = [E_{A,B}^*(t)/a]^{1/2} , \tag{5}$$

where the level density parameter a is taken as $M_{A,B}(t)/10$, $M_{A,B}(t)$ being the dynamical mass numbers of the reactants at any instant of time t. The dynamical change in the intrinsic nucleon momentum distributions is incorporated in the calculations as finite-temperature Fermi distribution, as in Ref. [9]. Intrinsic nucleon velocity and the point of transfer on the window plane are generated randomly at every time step along the trajectory.

The exchanged nucleon during its passage through the medium of the recipient may be completely absorbed in the nucleus by way of successive two-body collisions and dump its full energy and momentum, or it may pass through the nucleus undisturbed with a probability $e^{-d/\lambda}$, where d is the path length and λ is the energy-dependent mean free path, calculated from the nucleon-nucleus optical potential [9]. These nucleons are finally emitted in the continuum provided their energies satisfy the following energy condition:

$$\varepsilon_b > U + V_C , \tag{6}$$

where U is the depth of the nuclear potential and V_C is the Coulomb barrier (zero for neutrons). The emission probability $e^{-d/\lambda}$ is calculated and is tested against a random number. If the probability is greater than or equal to the random number and the energy conditions mentioned earlier [Eq. (6)] are satisfied, a particle is emitted in the continuum; otherwise, the exchanged particle is completely absorbed in the system. These emitted particles constitute one-body or primary PEP's.

If the calculations are stopped at this stage then it is assumed that, in case the exchanged particle suffers two-body collisions in the recipient, it is completely absorbed and there is no PEP emission. However, in the intermediate energy domain, for the first two-body collision, one or both of the scattered nucleons may have sufficient energy to be emitted in the continuum provided the energy condition [Eq. (6)] is satisfied. These emitted particles are termed as secondary PEP's or two-body PEP's. For the emission of secondary PEP's, we follow the identical procedure as is done in the case of primary PEP's, i.e., we calculate the emission probabilities e^{-d_i/λ_i}, $i=1,2$ (d_i's being the distances traveled by the scattered nucleons in the recipient and λ_i's the corresponding mean free paths) and test them against the random numbers.

The total energy carried away by PEP's (primary plus secondary) $\varepsilon_{\rm PEP}$ is given by

$$\varepsilon_{\rm PEP} = \sum_i (E_i - U) , \tag{7}$$

where E_i is the energy of the nucleon in the medium and the summation is over the number of emitted nucleons in an event. For the primary PEP's, $E_i = \varepsilon_b$ and for the secondary PEP's, E_i's are calculated using standard two-body kinematics, assuming that the collisions are elastic with isotropic angular distribution in the center of mass of the colliding nucleons. Thus the particle absorption in the recipient may be reduced due to the emission of two-body PEP's. However, we do not consider further particle emission from sequential two-body collisions as they are not of much importance at the energies considered here.

At each time step, dynamical mass and charge numbers and excitation energies of the reactants as well as the velocities of the emitted nucleons are calculated. Finally the mass, charge, excitation energy, and velocity of the composite are calculated, using the appropriate conservation laws. We present here the results of the calculations for an impact parameter $b = 0.5$ fm (typical of central collisions). For any other fusion trajectories, the average results do not change significantly.

B. Evaporation phase

The incompletely fused composite (IFC) obtained from the previous phase has its mass $A_{\rm IFC}$ charge $Z_{\rm IFC}$, excitation energy $E_{\rm IFC}^*$, and velocity $\mathbf{v}_{\rm IFC}$ given by

$$A_{\rm IFC} = A_P + A_T - N_{\rm PEP} , \tag{8a}$$

$$Z_{\rm IFC} = Z_P + Z_T - N_{\rm PEP}^{\rm proton} , \tag{8b}$$

$$\mathbf{v}_{\rm IFC} = (\mathbf{P}_{\rm in} - \mathbf{P}_{\rm PEP})/(m A_{\rm IFC}) , \tag{8c}$$

$$E_{\rm IFC}^* = E_{\rm lab} - \tfrac{1}{2} m A_{\rm IFC} v_{\rm IFC}^2 - \varepsilon_{\rm PEP} , \tag{8d}$$

where $N_{\rm PEP}$ is the total number of PEP's (proton + neutron) $N_{\rm PEP} = N_{\rm PEP}^{\rm proton} + N_{\rm PEP}^{\rm neutron}$, and A_P, Z_P, A_T, and Z_T are the mass and charge number of the projectile and the target, respectively. $\mathbf{P}_{\rm in}$ is the incoming moment, $\mathbf{P}_{\rm PEP}$ is the momentum carried away by PEP's, and $E_{\rm lab}$ is the incident energy. This composite is allowed to decay (forming the same event) according to the binary sequential decay process. Detailed description of the binary sequential decay process is already available in the literature [10–12]. Here we give only the basic features. The fragmentation of the initially excited nucleus proceeds along a chain of binary decays of the successive nuclei which are generated at the previous step. In this way, the fragments progressively lose their excitation energy and fly apart in space under the effect of the kinetic energy acquired from the Coulomb energy between the fragments at the time of separation. The scenario of multisequential decay is simulated event by event, by means of a Monte Carlo technique [12].

A fragment j with A_j nucleons and Z_j protons may decay into two fragments i and $(j-i)$ with rate per unit time given by

$$W_{j\to(j-i)+i}=\int_{E_C(j-i;i)}^{E_{\max}} dE\, d^2\pi_{ji}/dE\, dt \ , \tag{9a}$$

where

$$E_{\max}=E_j^*+B_j-(B_i+B_{j-i}) \ . \tag{9b}$$

E_j^* is the excitation energy of the fragment j; B_i, B_{j-i}, B_j are the binding energies of the different fragments; and $E_C(j-i;i)$ and the Coulomb barrier between the fragments i and $(j-i)$. The transition rate per time and energy units is written as

$$\frac{d^2\pi_{ji}}{dE\, dt}=\frac{1}{\pi^2\hbar^3}\frac{\bar{J}_i\bar{J}_{j-1}}{\bar{J}_j}E\sigma_{ji}\frac{\mu}{\omega_j(E_j^*)} \times\int_0^{\varepsilon^*} d\varepsilon\,\omega_{j-i}(\varepsilon)\omega_i(\varepsilon^*-\varepsilon) \ , \tag{10}$$

where $\bar{J}_k=2J_k+1$ ($\bar{J}_k$ is the average spin of the excited cluster k), σ_{ji} the fusion cross section for $i+(j-i)\to j$, μ the reduced mass of the system, $\omega_k(\varepsilon)$ the level density at energy ε of fragment k, and $\varepsilon^*=E_{\max}-E$. More details about the different quantities can be found in Ref. [10].

The decay of the incompletely fused composite $(A_{\rm IFC},Z_{\rm IFC})$ starts with a temperature $T_{\rm IFC}$ obtained from the excitation energy $E^*_{\rm IFC}$ using Eq. (5). At any given step of the decay process the number of fragments of a given type j, their velocities and kinetic energies with respect to the initial reference frame, as well as their excitation energies, are known. For each fragment j one chooses a decay channel $j\to(j-i)+i$ and the total kinetic energy $E_{\rm kin}$ $[E_C(j-i;i)\le E_{\rm kin}\le E_{\max}]$ of the emerging fragments by means of probability laws obtained from $W_{j\to(j-i)+i}$ and $dW_{j\to(j-i)+i}/dE$ respectively. The angle of i and $(j-i)$ within the reference frame attached to j is chosen at random over the whole solid angle 4π. Velocities $\mathbf{v}_i$ and $\mathbf{v}_{(j-i)}$ and kinetic energies $E^{(i)}_{\rm kin}$, $E^{(j-i)}_{\rm kin}$ are calculated under the constraint of momentum conservation and the excitation energies are obtained from energy conservation

$$B_j+E_j^*=E_{\rm kin}+E_i^*+E_{j-i}^*+B_i+B_{j-i} \ , \tag{11}$$

by assuming that the remaining excitation energy is shared by the fragments in proportion to their masses. Finally, the velocities of the fragments in the reference frame of the incompletely fused composite $(A_{\rm IFC},Z_{\rm IFC})$ are computed and the total conversation is checked. The same procedure is applied to all existing fragments. The simulation proceeds up to the point where all the fragments present in the system can no longer decay.

The decay process yields all types of clusters smaller than the initial composite. However, we pick up only nucleons, alphas, and the heaviest residue in each event for the present calculations. The number of nucleons and alphas emitted and mass of the residues are determined by the initial excitation and the dynamics of the decay process.

III. RESULTS AND DISCUSSIONS

We have studied the representative systems ^{40}Ar+^{24}Mg and ^{40}Ar+^{13}C at 1100 MeV and have calculated the relevant physical observables which are compared with the respective experimental observations.

A. Time evolution

In Fig. 1 (upper half) we plot the average nucleon loss from the projectile and the target versus time along the trajectory in the preequilibrium phase of the reaction ^{40}Ar+^{24}Mg at 1100 MeV. Our calculations show that the target (the lighter partner in the reaction) loses more particles as compared to the projectile (heavier partner). This is in accordance with phenomenological analysis of the intermediate energy nucleus-nucleus collisions by Morgenstern *et al.* [1]. Moreover, it is observed that at time $t\ge 50$ fm/c there is no further nucleon loss through preequilibrium particle emission. The projectile and target temperature T evaluations as a function of time are shown in the lower half of Fig. 1. It appears that the two

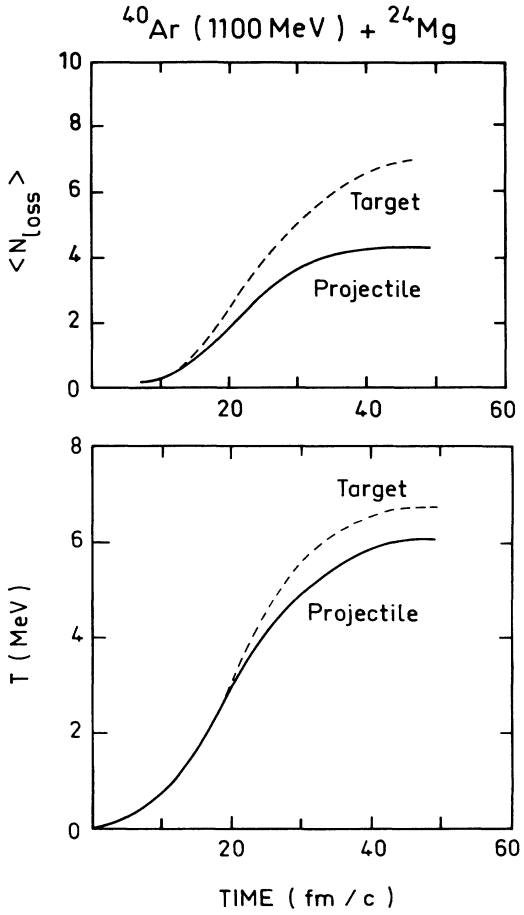

FIG. 1. (Upper half): Total number of nucleons lost from the target and the projectile during the preequilibrium phase of the reaction as a function of time for the system ^{40}Ar+^{24}Mg at $E_{\rm lab}=1100$ MeV. (Lower half): Projectile and target temperature as a function of time.

temperatures remain close together and saturate at $t \sim 50$ fm/c. So, in the present model, up to this time the reaction is in the preequilibrium phase; beyond this time the incompletely fused composite formed at the end of preequilibrium stage is assumed to be fully equilibrated which subsequently undergoes binary sequential decay. This time corresponds to internuclear distance of ~ 2 fm where we stop the trajectory calculation. The system $^{40}Ar + ^{13}C$ follows the similar type of time evolution (not shown in Fig. 1).

B. Inclusive fragment charge distribution

Inclusive fragment charge distributions for the reaction $^{40}Ar + ^{13}C$ at 1100 MeV have been plotted in Fig. 2 for the fragment detection angles of 5° and 8° along with the experimental data [8]. It is seen that the theoretical calculations are in good agreement with the respective experimental data. However, the peaks of the calculated distributions are shifted on the higher side by 1–2 charge units, as compared to the experimental peaks. The position of the peak depends on the charge and excitation energy of the incompletely fused composite. The inclusion of complex particles emission at the preequilibrium phase would definitely affect both of these quantities and this would bring the desired change in the peak positions as indicated in Ref. [14], where it has been shown in an indirect way that the complex particle emission in the preequilibrium stage does shift the inclusive mass distributions towards lower masses.

C. Exclusive proton and alpha-particle yields

In Figs. 3 and 4 we show the calculated exclusive proton yield (energy integrated) at 25° and 165° respectively for the reaction $^{40}Ar + ^{24}Mg$ at 1100 MeV versus the mass of the coincidental residues detected at 8.5° along with the experimental data [14]. The agreement achieved between the experimental results and the theoretical results (solid line histogram) is good. The experimentally observed peak is well reproduced. The dashed line histograms in Figs. 3 and 4 correspond to the contributions to the exclusive proton yield from the evaporation stage only. It is observed that at the forward angle (Fig. 3), the contribution from the evaporation stage is quite sizable, whereas at the backward angle (Fig. 4), the contribution to the proton yield from the evaporation stage is significantly smaller. So, the protons observed at the backward angle originate mainly during the preequilibrium phase of the reaction.

In Fig. 5, we display the calculated exclusive proton and alpha yields (energy integrated) for the reaction $^{40}Ar + ^{13}C$ at 1100 MeV in coincidence with the fragments detected at 5° along with the experimental data [8]. The upper and middle parts of the figure correspond to protons detected at $\pm 30°$ and $\pm 125°$ respectively and the lower part corresponds to alpha particles detected at $\pm 30°$. Positive (negative) angles correspond to the protons or alphas detected on the same (opposite) side of the fragment detector with respect to the beam direction. In all the cases, the calculations reproduce the experimental trends and the peak positions fairly well.

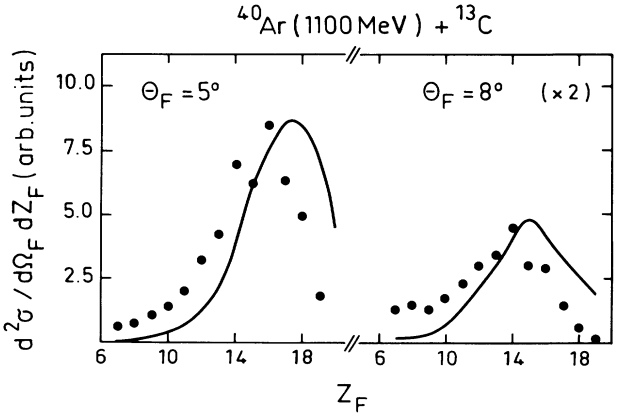

FIG. 2. Inclusive fragment yield as a function of fragment charge (Z_F) detected at $\theta_F = 5°$ and 8° for the reaction $^{40}Ar + ^{13}C$ at $E_{lab} = 1100$ MeV. Filled circles are the experimental data [8] and the solid curves correspond to the results of the present calculation.

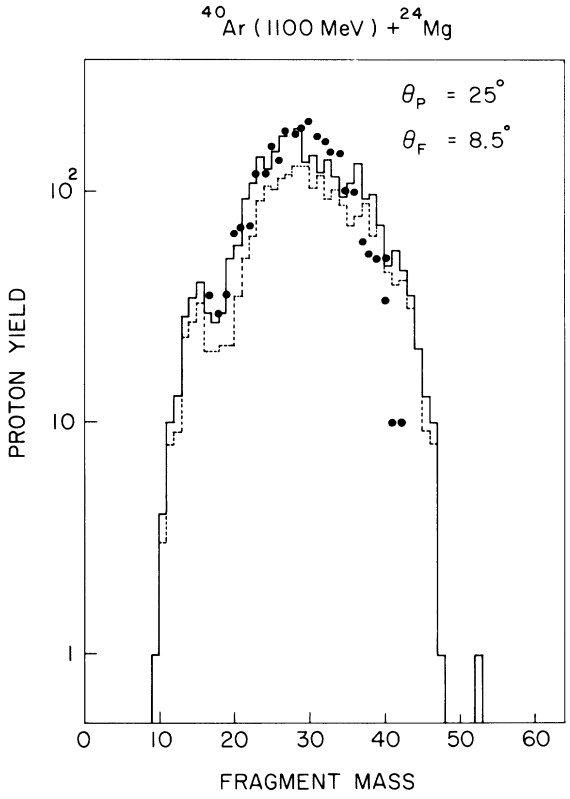

FIG. 3. Exclusive (integrated) proton yield as a function of residue mass for the protons detected at $\theta_P = 25°$ in coincidence with residues at $\theta_F = 8.5°$ for the reaction $^{40}Ar + ^{24}Mg$ at 1100 MeV. Filled circles are the experimental data [14]. The solid histogram corresponds to the calculated total (preequilibrium plus evaporation) proton yields and the dashed line histogram corresponds to the calculated proton yield from the evaporation phase only.

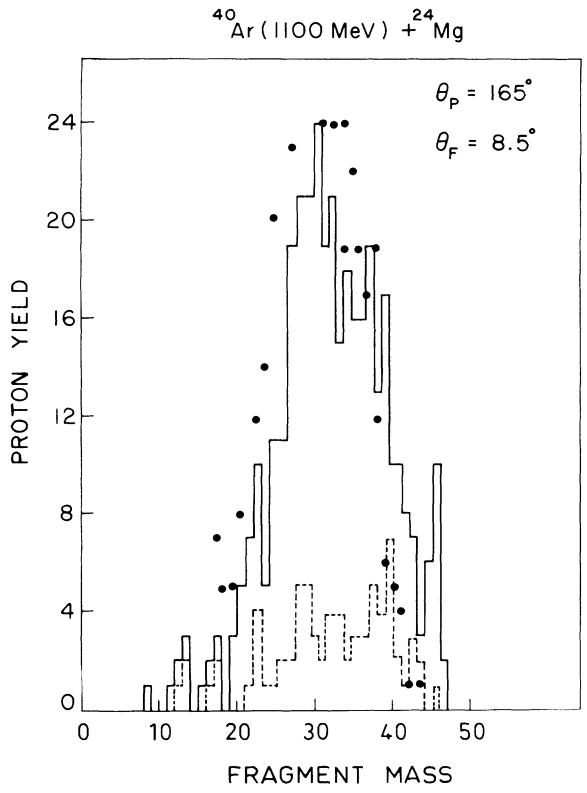

FIG. 4. Same as Fig. 3 for the protons detected at 165°.

D. Average velocity of the emitted protons

We have calculated the average velocity of the protons emitted at backward angles $-125°$ and $-165°$ for the reaction $^{40}Ar+^{24}Mg$ at 1100 MeV as a function of residue mass measured in coincidence with the residues detected at 8.5° and confront our calculated results with the experimental data [15] (Fig. 6). There is good agreement between the calculated and the experimental results. The increase in the average proton velocity with increase in mass of the residue can be understood as follows. In an inverse kinematical reaction the backward particle emission is predominantly from the preequilibrium phase of the reaction. Therefore, the composite formed after the preequilibrium phase through emission of more energetic particles would yield larger mass residues (less excitation energy in the composite) and vice versa, and hence the increase of average particle velocity with increase in residue mass.

E. Exclusive proton and alpha energy distributions

In Figs. 7 and 8 we have plotted the calculated exclusive proton and α energy spectra, respectively, for the reaction $^{40}Ar+^{13}C$ at 1100 MeV in coincidence with the residues measured at 5° along with the respective experimental data [8]. Figure 7 corresponds to the proton spectra calculated for the angles 15°, ±30°, and ±125°. The calculated proton spectra agree well with the experimental spectra at the forward as well as the backward angles. The slopes of the experimental spectra are well reproduced. However, at forward angles the calculated proton yield is less compared to the experimental yield at low energies. The departure at low proton energies between the calculations and the data may be due to the contributions from the targetlike fragments produced in peripheral collisions, which have not been considered in the present calculations. This effect could unbalance the preequilibrium to evaporation yield ratio as discussed to some extent in Ref. [14].

In Fig. 8 we have plotted the calculated exclusive α-particle spectra for 15° and ±30° angles in coincidence with the residues detected at 5° along with the experimental data [8]. The calculated spectra at all the angles agree well with the experimental spectra, though the tails of the spectra are not reproduced. In our model, the preequilibrium phase is constrained only to the nucleon degrees of freedom as there is no simple way known to include the cluster emission, like α particle. Hence the high energy

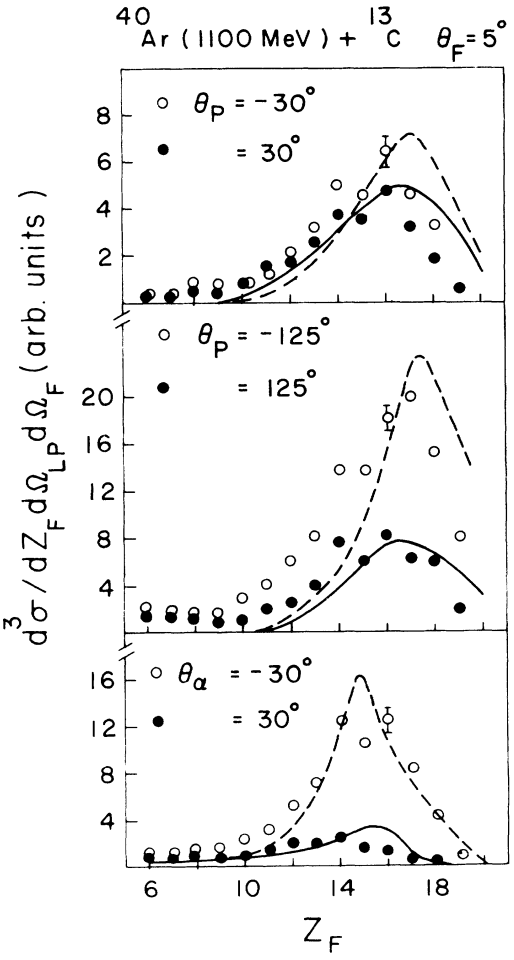

FIG. 5. Exclusive energy integrated yields for the protons detected at $\theta_P = \pm 30°$ (upper), ±125° (middle), and for the α particles detected at $\theta_\alpha = \pm 30°$ (lower) in coincidence with the residues at 5° for the system $^{40}Ar+^{13}C$ at 1100 MeV. Filled (open) circles are the experimental data and solid (dashed) curves are the theoretical results for positive (negative) angles, respectively. The meaning of positive (negative) angles is described in the text.

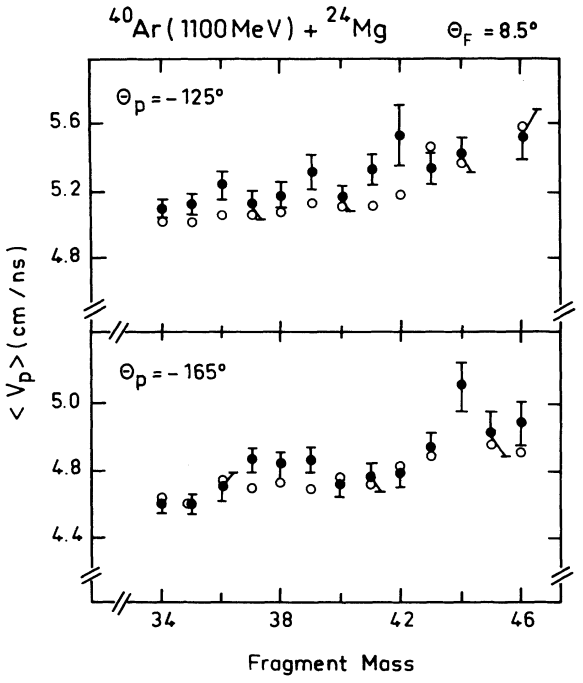

FIG. 6. Average velocity ($\langle V_P \rangle$) of the protons emitted at $\theta_P = -125°$ (upper half) and $-165°$ (lower half) as a function of mass of the residues detected at $\theta_F = 8.5°$ for the reaction $^{40}Ar + ^{24}Mg$ at 1100 MeV. Open and filled circles correspond to the present calculations and the experimental results, respectively.

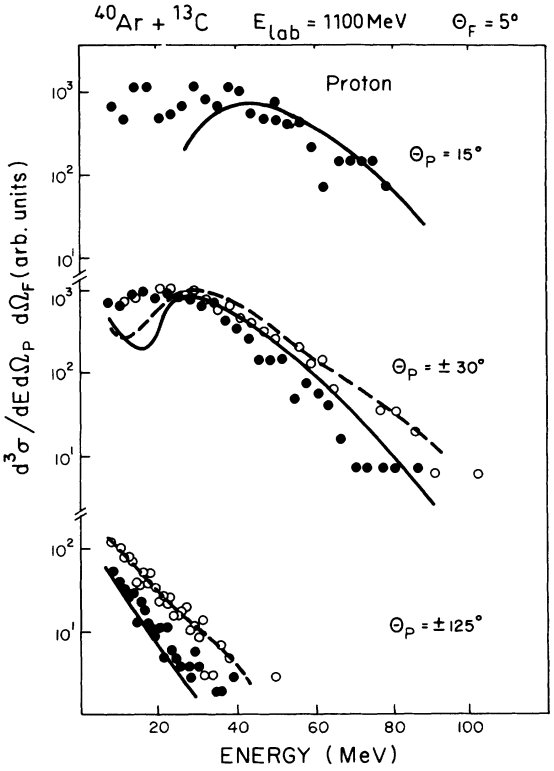

FIG. 7. Exclusive proton energy distribution at $\theta_{LP} = 15°$ (upper), $\pm 30°$ (middle), and $\pm 125°$ (lower) for the reaction $^{40}Ar + ^{13}C$ at 1100 MeV obtained in coincidence with the residues detected at $\theta_F = 5°$. Open and filled circles correspond to the experimental data for the positive and negative angles, respectively. Solid and dashed curves are the results of the present calculations for the positive and negative angles, respectively.

tails in the α-particle spectra which may have come from the preequilibrium α-particle emission cannot be reproduced in our model. From the good fit of the calculated spectra with experimental spectra, it can be inferred that the α emission is mainly from the binary sequential decay phase of the reaction. The calculated spectrum at 15° reproduces nicely the double peak which corresponds to the two kinematical solutions for the α-particle emission in this reaction [8].

IV. SUMMARY AND CONCLUSIONS

In summary, we have developed a dynamical prescription for the study of incomplete fusion processes in intermediate energy heavy ion reactions. The calculations are comprised of two parts: (i) The calculation of the initial preequilibrium phase, followed by (ii) the calculation for the evaporation phase. The calculations have been performed on an event-by-event basis using a Monte Carlo simulation technique and are parameter free. The excited primary composite formed after the initial preequilibrium phase is assumed to be thermally equilibrated. Typical time taken by the system to reach the end point of the preequilibrium phase (after which the thermally equilibrated primary composite is assumed to be formed) is found to be ~ 50 fm/c. Similar results are also obtained from the Landau-Vlasov calculations. The inclusive fragment charge distributions predicted from the present model are found to be in fair agreement with the corresponding experimental values, except that the peaks of

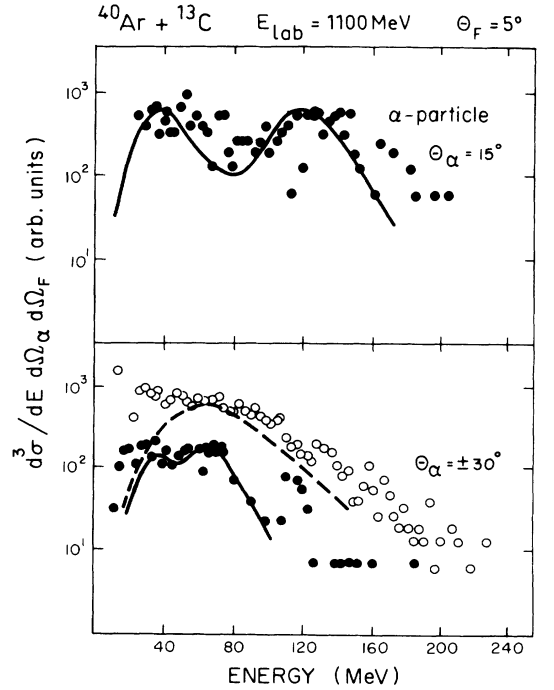

FIG. 8. Same as Fig. 7 for the α particles at $\theta_{LP} = 15°$ (upper) and $\pm 30°$ (lower). All the symbols have the same meaning as in Fig. 7.

the calculated charge distributions are shifted by 1–2 units on the higher side as compared to the experimental values. The peak of the charge distribution generally depends upon the excitation energy and the charge of the incompletely fused composite. Therefore, the inclusion of complex particles (like α particles) emission in the preequilibrium phase may have improved the quality of the fit. Exclusive proton yields as a function of fragment mass and charge have been quite well reproduced at all angles considered, both forward and backward. At the backward angles proton yield is dominantly due to the preequilibrium emission, whereas at the forward angles the proton yield from the evaporation phase has a sizable contribution. The exclusive proton emission spectra at both forward and backward angles predicted from the present model are in very good agreement with the respective experimental measurements for both the systems $^{40}Ar+^{24}Mg$ and $^{40}Ar+^{13}C$. However, the α emission spectra measured for the system $^{40}Ar+^{13}C$ at 1100 MeV show a high energy tail which extends beyond the present theoretical predictions. Since this high energy tail of the α emission spectra is most likely to have a preequilibrium origin, it is natural that the present model, where preequilibrium emissions of only nucleons are considered, would fall short of explaining the high energy tail of the alpha particles. Thus, it would be worthwhile to incorporate the emission of complex particles (at least up to α's) in the preequilibrium phase of the present model to be able to have a better agreement with the experimental data.

Hence, the present model, though having certain limitations, is able to explain reasonably well most of the experimentally observed quantities in intermediate energy incomplete fusion reactions and is a viable candidate for the reaction mechanism dominant in this energy domain.

ACKNOWLEDGMENTS

The authors would like to thank J. Richert for helpful and illuminating discussions. One of the authors (K.K.) acknowledges useful discussions with S. K. Samaddar. He also acknowledges the hospitality extended to him during his stay at CRN de Strasbourg.

[1] H. Morgenstern, W. Bohne, K. Grabisch, D. G. Kovar, and H. Lehr, Phys. Lett. **113B**, 463 (1982).

[2] J. Galin, H. Oeshler, S. Song, B. Borderie, M. F. Rivet, I. Forest, R. Bimbot, D. Gardes, B. Gatty, H. Guillemot, M. Lefort, B. Tamain, and X. Tarrago, Phys. Rev. Lett. **48**, 1787 (1982).

[3] For a review see, for example, D. Guerreau, in *Nuclear Matter and Heavy Ion Collisions,* edited by M. Soyeur, H. Flocard, B. Tamain, and M. Porneuf (Plenum, New York, 1989).

[4] E. Holub, D. Hilscher, G. Ingold, U. Jahnke, H. Orf, H. Rossner, W. P. Zank, W. U. Schroeder, H. Gemmeke, K. Keller, L. Lassen, and W. Lucking, Phys. Rev. C **33**, 143 (1986).

[5] B. A. Remington, G. Caskey, A. Galonsky, C. K. Gelbke, L. Heilbronn, J. Heltsley, M. B. Tsang, F. Deak, A. Kiss, Z. Seres, J. Kasagi, and J. J. Kolata, Phys. Rev. C **34**, 1685 (1986).

[6] C. Block, W. Benenson, A. I. Galonsky, E. Kashy, J. Heltsley, L. Heilbronn, M. Lowe, R. J. Radtke, B. Remington, J. Kasagi, and D. J. Morrissey, Phys. Rev. C **37**, 2469 (1988).

[7] J. C. Steckmeyer, G. Bizard, R. Brou, P. Eudes, J. L. Laville, J. B. Natowitz, J. P. Patry, B. Tamain, A. Thiphagne, H. Doubre, A. Peghaire, J. Peter, E. Rosato, J. C. Adloff, A. Kamili, G. Rudolf, F. Scheibling, F. Guilbault, C. Lebrun, and F. Hanappe, Nucl. Phys. **A500**, 372 (1989).

[8] M. Zahar, A. Malki, M. Bozin, P. Wagner, F. Rami, J. P. Coffin, G. Guillaume, F. Jundt, P. Fintz, B. Rastegar, D. Rebreyend, F. Merchez, J. Mistretta, and S. Kox, Z. Phys. A **339**, 465 (1991).

[9] S. Bhattacharya, K. Kirshan, J. N. De, and S. K. Samaddar, Phys. Rev. C **37**, 2916 (1988).

[10] C. Barbagallo, J. Richert, and P. Wagner, Z. Phys. A **324**, 97 (1986).

[11] J. Richert and P. Wagner, Nucl. Phys. **A466**, 132 (1987).

[12] J. Richert and P. Wagner, Nucl. Phys. **A517**, 399 (1990).

[13] K. Krishan, S. Bhattacharya, J. N. De, and S. K. Samaddar, Phys. Lett. B **211**, 269 (1988).

[14] A. Malki, J. P. Coffin, G. Guillaume, F. Jundt, K. Krishan, F. Rami, P. Wagner, P. Fintz, M. Zahar, M. Gonin, B. Heusch, M. Ohta, B. Rastegar, D. Rebreyend, F. Merchez, J. Mistretta, and S. Kox, Z. Phys. A **339**, 283 (1991).

[15] A. Malki, Ph.D. thesis, Universite de Strasbourg, 1990.